Int. J. Heat Mass Transfer. Vol. 24, pp. 507–519

0017-9310/81/0301-0507 $02.00/0

TURBULENT HEAT TRANSFER COEFFICIENTS AND FLUID FLOW PATTERNS ON THE FACES OF A CENTRALLY POSITIONED BLOCKAGE IN A DUCT

E. M. SPARROW, M. MOLKI and S. R. CHASTAIN

Department of Mechanical Engineering, University of Minnesota, Minneapolis, MN 55455, U.S.A.

(*Received* 19 *May* 1980 *and in revised form* 21 *August* 1980)

Abstract—Experiments encompassing both heat-transfer measurements and flow visualization were performed for turbulent flow in a square duct whose cross section was partially obstructed by a centrally positioned transverse blockage. Heat-transfer coefficients were obtained for both the upstream and downstream faces of the blockage element. The flow visualization, performed with the oil-lampblack technique, revealed the presence of three stagnation zones on the upstream face. The downstream face is washed by highly complex recirculation zones, characterized by sidewise fluid motions (along the span of the blockage). Heat-transfer coefficients on the upstream face generally increase with the square root of the Reynolds number; at a given mass flow, higher coefficients are in evidence at smaller blockage heights. The downstream-face coefficients display a complex dependence on both the blockage height and the Reynolds number. In the main, for the Reynolds number range investigated, the upstream-face coefficients are greater than the downstream-face coefficients. Comparisons with the literature showed that the coefficients for a centrally positioned blockage exceed those for a wall-attached blockage by as much as a factor of two.

NOMENCLATURE

- $\mathscr{D}$, naphthalene–air diffusion coefficient;
- H, side of square duct, Fig. 1;
- h, height of blockage element, Fig. 1;
- K, mass-transfer coefficient, $\dot{m}/\rho_{nw}$;
- $\dot{m}$, rate of mass transfer per unit area;
- Nu, Nusselt number;
- Re_{duct}, duct Reynolds number, $\bar{u}H/\nu$;
- Sh_H, Sherwood number, $KH/\mathscr{D}$;
- Sh_h, Sherwood number, $Kh/\mathscr{D}$;
- $\bar{u}$, average velocity in duct;
- $\bar{u}_{gaps}$, average velocity in gaps above and below blockage;
- $\dot{w}$, mass flow rate in duct.

Greek symbols

- ν, kinematic viscosity;
- ρ, density;
- ρ_{nw}, naphthalene vapor density at plate surface.

INTRODUCTION

WHEN a fluid flow encounters a transverse blockage, the flow experiences difficulty in following the contour of the blockage, especially on downstream-facing portions of the blockage element. Generally, the mainstream separates from the downstream face of the blockage, and the space between the face and the mainstream is occupied by a recirculating flow. The presence of a separated region filled with a recirculating fluid has a profound effect on heat transfer, both at the blockage element itself and at downstream-positioned surfaces which may be washed by the recirculating flow. The recirculating flow is particularly complex when the geometry of the blockage is three dimensional.

The fluid flow on the upstream face of a blockage element is usually less complex than that on the downstream face, although separation zones may also occur on the upstream face. There is usually a stagnation line or zone on the upstream face, and for three-dimensional geometries there may be more than one stagnation zone. These features strongly affect the upstream-face heat-transfer characteristics.

The present investigation is concerned with the heat transfer and fluid flow characteristics associated with a blockage element which partially obstructs the flow cross section of a square duct. Schematic diagrams of the blockage element and its positioning in the duct are presented in the left-hand portion of Fig. 1, respectively in cross sectional view (upper diagram) and side view (lower diagram). As seen there, the blockage is a thin plate which is centrally positioned in the height of the duct and spans the duct width.

The plate height is denoted by h, while the duct height is H (equal to the side of the square). The blockage ratio h/H was varied parametrically during the course of the research, ranging from a minimum value of 1/6 (moderate blockage) to a maximum of 2/3 (large blockage). In addition, at each blockage ratio, the Reynolds number was varied over a range encompassing about a factor of ten (the specific values of the Reynolds number depend on the selected definition).

The research is focused on the fluid flow about the blockage and on the heat-transfer coefficients on the upstream and downstream faces. The flow field was visualized by means of the oil-lampblack technique, which exposed the streamline pattern in the fluid passing adjacent to the faces of the blockage element. Other features of the flow such as stagnation lines (and zones) and regions of recirculation were also made visible. The flow visualization was performed sep-

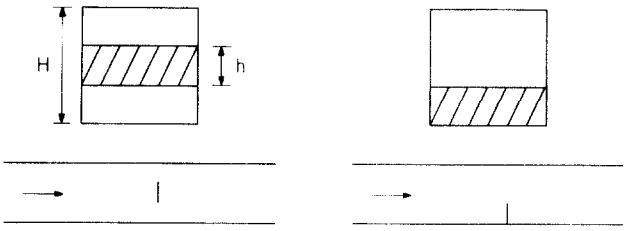

FIG. 1. Schematic diagram of a centrally positioned blockage element in a duct (left-hand diagram) and of the wall-attached blockage of [3] (right-hand diagram).

arately for the upstream and downstream faces.

The heat-transfer coefficients were determined by transforming measured mass-transfer coefficients in accordance with the well-established analogy between the two processes. Mass-transfer measurements were performed by employing the naphthalene sublimation technique. The transfer coefficients were separately determined for the upstream and downstream faces.

To provide perspective on the novel aspects of the physical problem, it is interesting to indicate the main features of the flow field which would be consistent with two-dimensional fluid mechanics. The upper diagram of Fig. 2 shows these features, which include the stagnation of the flow on the upstream face and the twin recirculation zones which stand aft of the downstream face. The projections of the respective streamlines on the upstream and downstream faces would yield the pattern that is indicated in the lower diagram of Fig. 2. This diagram shows a horizontal stagnation line, with upward-directed streamlines above and downward-directed streamlines below. The same pattern of streamline traces would be applicable to both the upstream and downstream faces.

The just-discussed flow pattern, while appropriate for two-dimensional conditions, is not consonant with the realities of the three-dimensional flow which is induced by the presence of the in-duct blockage. Deviations of the actual flow field from that pictured in Fig. 2 will be identified during the presentation of results. As will be seen there, the actual upstream-face flow patterns, although complex, can be readily rationalized. On the other hand, the flow patterns

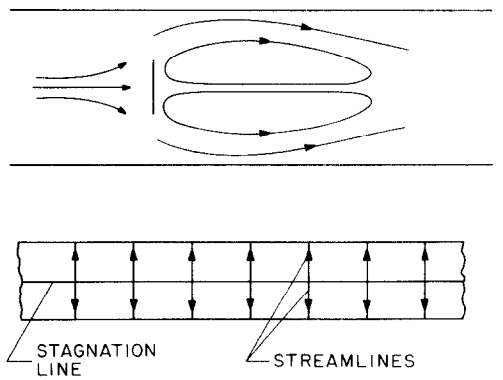

FIG. 2. Perceptions of the two-dimensional flow field about a transverse blockage in a duct.

adjacent to the downstream face are of a most remarkable and unexpected nature, and only tentative rationalizations can be given.

A search of the literature did not reveal any information on fluid flow patterns for three-dimensional in-duct blockages of the type considered here. With regard to heat transfer, there appear to be three relevant references. In [1], a wind tunnel study was performed in which a heated plate was positioned transverse to the flow. The wind tunnel had a 22 × 32 in rectangular cross section, and the plate spanned the entire 22 in tunnel dimension. Reynolds numbers, based on the wind-tunnel free stream velocity and the plate height (i.e. the h dimension of Fig. 1) extended from 110 000 to 420 000; these Reynolds numbers are more than an order of magnitude larger than those of the present study. Although the 21% blockage of the tunnel by the plate was undoubtedly a factor in the results of [1], blockage effects were not studied (only a single plate was employed), and the results were reported without reference either to blockage or to three-dimensional effects. The downstream-face heat-transfer coefficients reported in [1] will be compared with the present results later in the paper.

In [2], which is actually an Authors' Closure, some information is conveyed for upstream-face heat-transfer coefficients that were measured with the same apparatus as used in [1]. The given information is, however, not sufficient to enable comparisons to be made.

The last of the relevant heat-transfer references, [3], was a forerunner of the present study and dealt with a blockage which is wall attached as shown at the right (upper and lower diagrams) in Fig. 1. The central placement of the blockage for the present study, in contrast to the wall attachment of [3], brings about certain profound and readily identifiable changes in the flow pattern (plus others that are not so easily identifiable). For one thing, for the wall-attached blockage, there is a separation zone at the base of the front face of the blockage, where it meets the lower wall of the duct. There is no comparable separation zone for the central blockage, as will be demonstrated later. Second, for the wall-attached blockage, the recirculation zone is stabilized by the presence of the adjacent duct wall. For the central blockage, the recirculation region has very little contact with solid boundaries, so that it may be expected to be less stable. In [3], heat-

transfer coefficients are reported, but fluid flow patterns were not studied. Comparisons of the transfer coefficients will be made later.

THE EXPERIMENTS

Apparatus

The square duct used as the fluid flow environment for the blockage experiments was an adaptation of that of [3]. The flow cross section of the duct is a 44.35 × 44.35 mm (1.746 × 1.746 in) square, and the overall length of the duct is 2.75 m (9 ft) which corresponds to 62 hydraulic diameters. Aluminum bar stock, 9.53 mm (0.375 in) thick, carefully machined to close tolerances and hand polished to a high degree of smoothness, was used in the fabrication of the duct.

At a cross section situated 40 hydraulic diameters from the duct inlet, vertical slit-like access ports were provided in each of the side walls of the duct. These access ports enabled the naphthalene-coated blockage plates to be rapidly inserted (or removed) from the duct (time was of the essence to avoid extraneous sublimation mass transfer). The blocks which served to close the access ports were very carefully machined, with beveled edges to mate with corresponding bevels in the sides of the access ports. The blocks were designed to positively position and support the various blockage elements so that each element was centrally located along the height of the duct, as shown in Fig. 1.

The preselected 40-diameter length of duct upstream of the blockage was intended to serve as a hydrodynamic development section, with a view toward providing well-defined flow conditions at the blockage. In this regard, a square-edge inlet created by a large baffle plate was used to hasten the hydrodynamic development. Pressure taps deployed along the duct axis were employed to examine the degree of development, and measured pressure distributions indicated that a linear variation was established within about ten hydraulic diameters of the inlet.

The apparatus was operated in the open-circuit mode, with air being drawn into the duct from the laboratory room. After traversing the length of the duct, the air passed through a square-to-circular transition section and then to a calibrated rotameter, a control valve, and finally to the blower. The blower was situated outside the laboratory room so as not to affect the thermal environment and also to enable the discharge (i.e. the naphthalene-laden air) to be ducted outside the building.

Temperature control is important in naphthalene sublimation experiments because the vapor pressure of naphthalene, which provides the impetus for mass transfer, is very temperature sensitive (10% change of vapor pressure per °C at room temperature). The laboratory chosen for the experiments was temperature-controlled and also free of naphthalene vapor. The temperature of the air entering the duct was measured with an ASTM-certified thermometer having a smallest scale division of 0.1°F.

The rate of mass transfer from a naphthalene-coated blockage element during a data run was determined by direct weighings of the blockage element before and after the run. The mass was measured by a Sartorius 2432 analytical balance with a smallest scale division of 0.1 mg. Typically, the change of mass for a data run was 20 mg. Results for data runs made before and after recalibration of the balance differed by no more than did consecutively repeated runs (about 2%), thereby testifying to the precision of the calibration.

Four blockage element heights were employed during the course of the research. All blockage elements spanned the width of the duct (Fig. 1) and, in fact, the blockage elements extended into the two side walls. These extensions rested in recesses in the metal blocks which closed the access ports. The heights h of the blockage elements were chosen to be $H/6$, $H/3$, $H/2$, $2H/3$ (increments of $H/6$), where $H = 44.35$ mm (1.746 in). Six blockage elements were fabricated for each h/H ratio.

The blockage elements were metal plates chosen to have the minimum possible thickness consistent with the maintenance of flatness to at least 0.025 mm (0.001 in). Mild steel plates, 0.71 mm (0.028 in) thick, were found to be suitable.

With a view to separate determination of the upstream-face and downstream-face mass-(heat-) transfer coefficients, a naphthalene coating was applied to only one face of the metal substrate. The coating was confined to the exposed face (area $H \times h$), with no naphthalene being permitted on the portions of the metal plate which extended into the side walls of the duct.

The coating was applied by a combination of casting and machining. For the casting, the area to be coated was placed horizontal, facing upward, and framed by four metal bars. Molten naphthalene was poured into the thus-created open mold. After cooling and unmolding, the solidified naphthalene layer was carefully faced off to a final thickness of 0.28 mm (0.011 in) with a vertical milling machine fitted with a fly cutter attachment. The final surface finish was at least as good as a carefully machined metal surface.

Once the coatings were applied, the blockage elements were individually wrapped in impermeable plastic and sandwiched between glass plates, after which they were allowed to remain in the laboratory room for a minimum of twelve hours in order to attain thermal equilibrium.

Flow visualization

As noted earlier, the oil-lampblack technique was employed to enable visualization of the flow field adjacent to the faces of the blockage element. The use of this technique has been reported from time to time in the published literature, but its present application is a rather demanding one and merits some description.

Lampblack is a very fine black powder now primarily available as an ingredient of paint. It mixes

readily with oil, and the mixture, when brushed on a surface, produces a smooth, glossy-black coating. The fluidity of the mixture can be regulated by the selection of the viscosity of the oil and by the proportions of the oil and the lampblack powder. These proportions also have a significant effect on the degree of definition of the flow pattern that can be achieved with the method.

The general procedure for using the technique is to brush the oil-lampblack mixture on a surface and then to expose the surface to the airflow whose characteristics are to be studied. Ideally, under the action of the shear stresses exerted by the flow, the mixture will move along the surface, following the paths of the fluid particles that pass adjacent to the surface. These path lines will appear as streaks on the surface. In regions of low velocity (e.g. stagnation regions), the shear stresses are small and the mixture will remain stationary, so that such regions show themselves as black streak-free zones on the surface.

The degree of fluidity of the mixture is an especially relevant factor when the flow adjacent to a vertical surface is to be visualized, as is the case in the present investigation. In such a situation, the mixture will sag under the action of gravity, unless it is constituted so as to be stiff. However, if the velocities of the airflow adjacent to the surface are small, the stiff mixture will not respond and no path lines will be observed. Even if the use of a stiff mixture does not totally obscure the flow pattern, it may yield no information for those parts of a surface that are washed by moderate velocities, and only in regions of high velocity (or high shear) will a pattern be visible. Thus, for stiff mixtures, the correct flow pattern will be displayed in those regions where a pattern is visible, but the absence of an observable pattern in other regions does not necessarily mean that those regions are no-flow regions.

The foregoing paragraph suggests some of the special difficulties encountered in employing the oil-lampblack technique in the physical situation under study here. These difficulties were especially in evidence for the downstream face of the blockage element, where there are large variations of the shear stress across the face.

To facilitate the visualization, a number of oils of various viscosities were assembled, and numerous trial mixtures were employed in preliminary visualization runs. These trials provided guidance for the adopted operating procedure, which will now be described. For all visualization runs, both trial and final, the face under study (i.e. upstream or downstream) was coated with white, plasticized contact paper in order to provide the highest possible contrast for the black streak lines induced on the plate surface by the flow.

In order to obtain the clearest possible patterns, all of the final visualization runs were made at the highest Reynolds number studied, namely, a duct Reynolds number of about 30 000. From the preliminary runs, it was found that the flow patterns observed at this Reynolds number persisted at all the Reynolds numbers for which patterns could be obtained. These encompassed Reynolds numbers down to about half of the aforementioned 30 000.

The general approach for the downstream face was to make runs both with very stiff mixtures and with intermediate mixtures. The stiff-mixture runs were of relatively long duration, 0.5–0.75 h, and yielded remarkably sharp and clearly defined flow patterns in the regions of high shear. However, there were no streak lines visible in regions of low shear. The intermediate-mixture runs were of shorter duration (5–10 min). These runs yielded little or no detail in regions of high shear, since most of the mixture had been scrubbed from the surface by the airflow. However, very good resolution was obtained in regions of moderate and low shear.

For the upstream face, it was found possible, after a large number of trials, to find a mixture which would display all aspects of the flow pattern.

Photographic examples of the observed flow patterns will be presented shortly in the Results section of the paper. A systematic presentation of the flow patterns will be made via painstakingly prepared sketches. These sketches combine information from numerous data runs (e.g. for both stiff and intermediate mixtures) and, therefore, convey more complete information than would be conveyed by individual photographs.

RESULTS AND DISCUSSION

The presentation of results will be subdivided into two main sections, respectively for the fluid flow patterns and for the heat (mass) transfer. The flow patterns will be presented first, with the heat transfer to follow.

Photographs of fluid flow patterns

Representative photographs of the fluid flow patterns are presented in Figs. 3 and 4, respectively for the upstream and downstream faces of the blockage element. As was noted earlier, these photographs are included in the paper to illustrate the type of information that is provided by the oil-lampblack technique — sketches based on direct visual observations of the plates will be used to convey all the available flow pattern information. Figure 3 is for the upstream face of the $h/H = 2/3$ plate. The streamline traces are remarkably sharp and portray a strongly three-dimensional flow field. The black regions, one at the center of the plate and the other two adjacent to the respective side walls, depict stagnation regions. Almost perfect symmetry is seen to prevail, and there is no evidence that any sagging of the oil-lampblack mixture took place.

Two photographs are shown in Fig. 4 to illustrate the different nature of the information obtained when stiff and intermediate oil-lampblack mixtures are employed for the downstream-face flow visualization. The upper photograph, corresponding to the stiff mixture, is for $h/H = 1/2$, while the lower photograph,

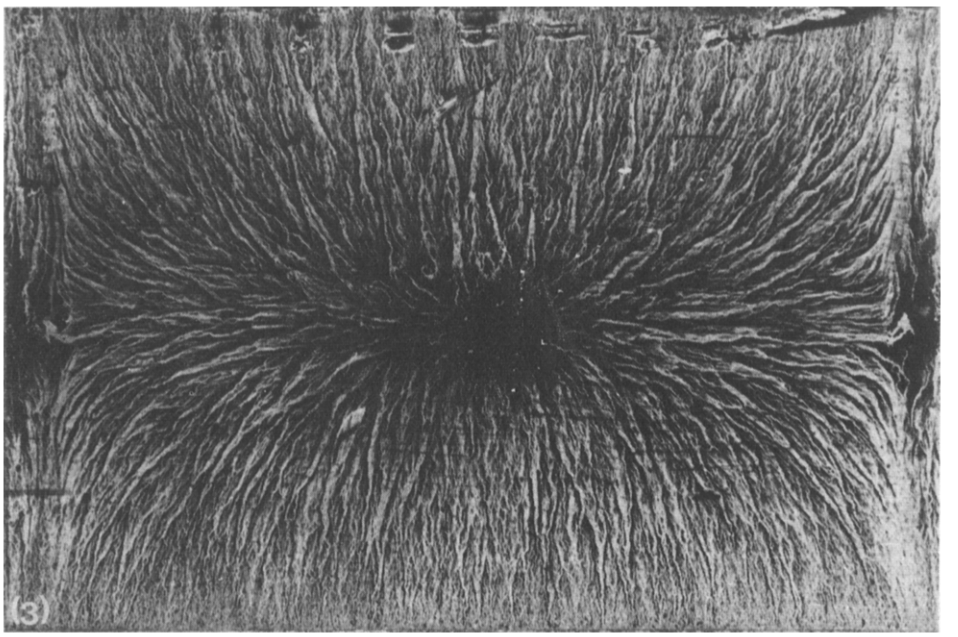

FIG. 3. Photograph of oil-lampblack visualization for the upstream face of the blockage, $h/H = 2/3$.

which corresponds to the intermediate mixture, is for $h/H = 2/3$.

The stiff-mixture photograph shows sharply etched horizontal flow lines issuing from a seemingly stationary vertical core. Flanking the zones of strong horizontal flow are black regions which, at face value, may be interpreted as being stationary. Sagging of the mixture is in evidence both within the flanking regions and adjacent to the lower surface of the plate. The sagging is responsible for a lack of symmetry in the vertical direction.

When a mixture of moderate stiffness is used, the visualization pattern (lower photograph of Fig. 4) appears quite different from that discussed in the preceding paragraph. The formerly sharply defined horizontal flow lines which emanate from the central vertical stagnation region now appear diffuse and ill-defined because the oil-lampblack mixture has been blown away from this highly active zone. Indeed, the central stagnation region now has a rather cellular appearance. However, the most remarkable difference between the upper and lower photographs of Fig. 4 can be seen in the regions adjacent to the side walls of the duct. What previously had seemed stationary is now revealed to be a wall-adjacent region of horizontal flow. These side bands of horizontal flow are separated from the strong inner zone of horizontal flow by heavy black vertical lines. As will soon be elaborated, these lines portray the stagnation which results from the collision of the oppositely directed inner and outer horizontal flows. Sagging of the mixture is in evidence at the bottom of the photograph. The two photographs of Fig. 4 affirm the desirability of using mixtures of different stiffness in order to make visible all aspects of the flow pattern.

Flow pattern presentation

Attention will now be turned to the flow patterns which were sketched from direct visual observations of the oil-lampblack traces on the upstream- and downstream-facing plates. The flow patterns adjacent to the upstream-facing plate are presented in Fig. 5, while those for the downstream face are shown in Fig. 6. To provide perspective for these results, it is useful to recall the expected patterns for a two-dimensional flow that were pictured in the lower diagram of Fig. 2. As seen there, the basic ingredients of the flow pattern, as would be shown by the oil-lampblack technique, are a horizontal stagnation line with vertical streamlines, upward-directed above the stagnation line and downward-directed below the stagnation line. This same pattern would be in evidence on both the upstream and downstream faces, even though the flow fields adjacent to these faces are different (see upper diagram of Fig. 2). It is clear from Figs. 5 and 6 that the actual flow patterns are markedly different from the two-dimensional perceptions that were just discussed.

Consideration may first be given to the upstream-face flow patterns of Fig. 5. There, arranged from top to bottom, are the results for $h/H = 1/3$, $1/2$ and $2/3$. Results for the $h/H = 1/6$ plate (the plate of least height) are not shown in the figure because, despite numerous attempts, an oil-lampblack mixture could not be found which would provide a clear flow pattern picture.

For all three plates, the flow pattern is characterized by a central stagnation zone from which issue outflowing streamlines. For the shortest of the three plates, the stagnation zone is wider than for the other cases, suggesting a kinship with the horizontal stagnation line of the two-dimensional case (Fig. 2, lower dia-

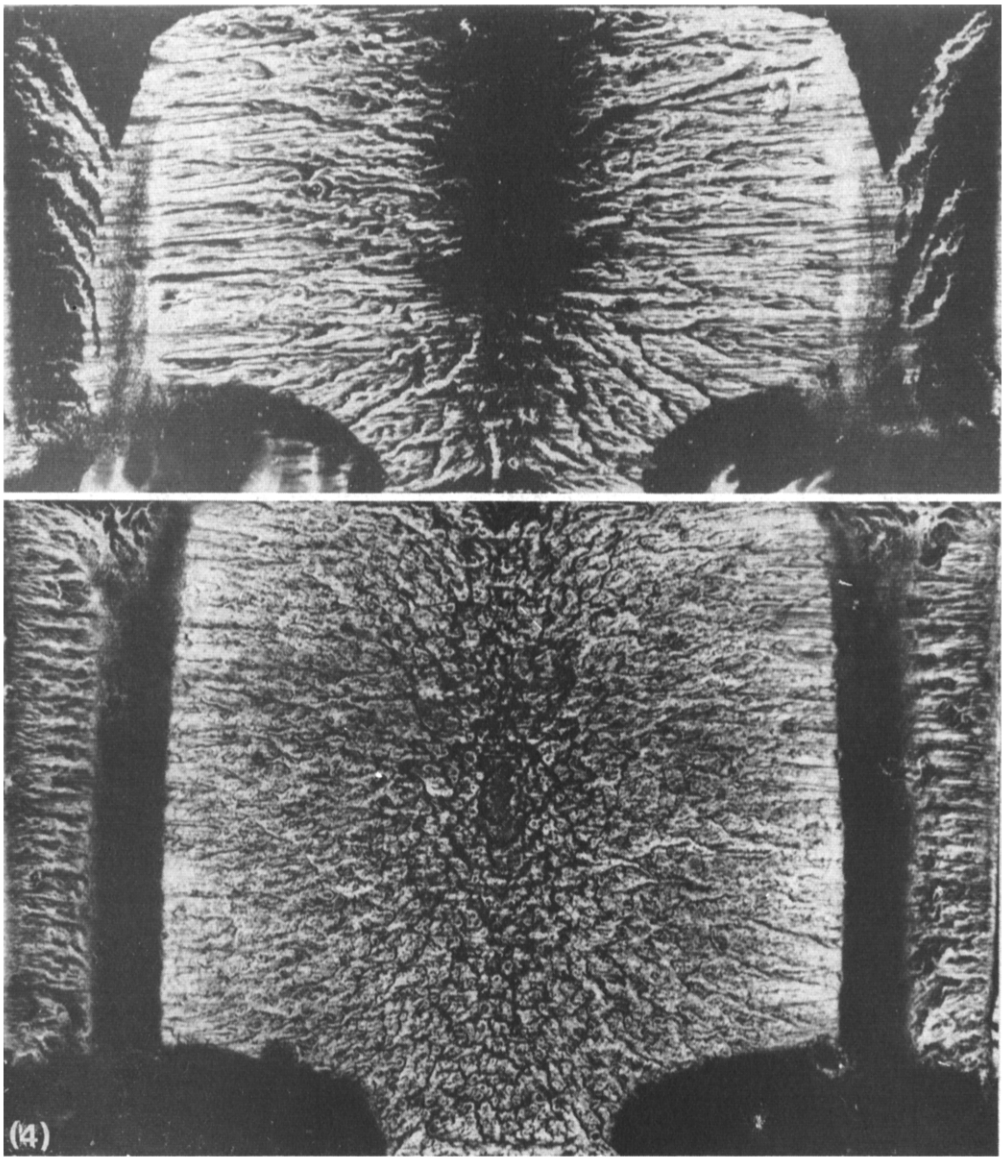

FIG. 4. Photographs of oil-lampblack visualization for the downstream face of the blockage, $h/H = 1/2$ (upper) and $h/H = 2/3$ (lower).

gram). As the plate height increases, the central stagnation zone becomes narrower and more nearly circular.

Some of the outflowing streamlines sweep over the top and bottom of the plate, while others are directed toward the side walls of the duct. These sidewise flows stagnate against the duct walls, as is evidenced by the black region situated adjacent to each side wall. The presence of the side walls causes a turning of the flow (either upward or downward), and the streamlines in the region of turning are reminiscent of the classical textbook picture of the streamlines of a stagnation point flow.

The sidewise flow is closely connected with a sidewise pressure gradient. This pressure gradient is set up because fluid passing through the central part of the duct cross section has a higher velocity than does fluid moving adjacent to the side walls. Therefore, when stagnated against the plate, the former attains a higher pressure than the latter.

Another relevant characteristic, which cannot be deduced from the figure but which has a strong logical basis, is the presence of a vortex adjacent to each side wall. To make this plausible, consider the sidewise flow as it approaches the wall. The flow impinges on the wall and "splashes", with part of the splashed flow moving upward, part moving downward, and part moving upstream (opposite to the direction of the mainstream flow). The upstream-moving portion collides with the main flow, and a vortex is created by the collision. Both the sidewise pressure gradient and the vortex play important roles in the downstream-face flow patterns, as will be discussed shortly.

As a final remark about Fig. 5, it may be concluded

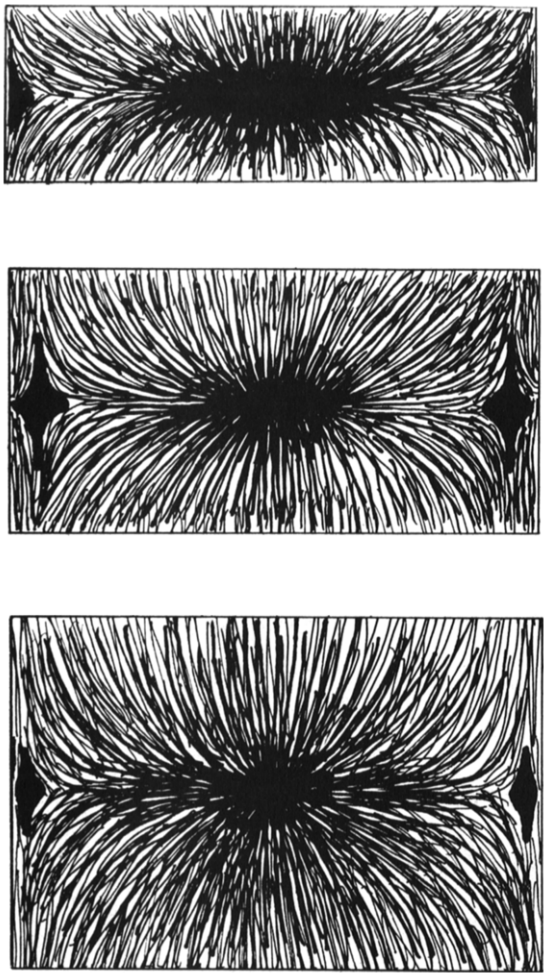

FIG. 5. Flow patterns on the upstream face of the blockage, top to bottom, $h/H = 1/3$, 1/2 and 2/3.

that the flow adjacent to the upstream face is eminently three-dimensional and that two-dimensional perceptions are far off the mark.

Attention will next be focused on the downstream-face flow patterns of Fig. 6. The upper diagram is for the $h/H = 1/3$ plate, the next two diagrams are for $h/H = 1/2$, and the lower diagram is for $h/H = 2/3$. For the shortest plate (upper diagram), the flow pattern in the central region is somewhat reminiscent of the two-dimensional expectation shown in the lower diagram of Fig. 2. There is a horizontal stagnation zone from which streamlines issue both upward and downward, but there are also sidewise-directed streamlines. Adjacent to both sides is a region of source-like outflow. The source streamlines move in a direction opposite to those issuing from the central horizontal stagnation zone. The collision of the two opposing flows creates the contoured vertical black bands, the presence of which is indicative of a region of very slow or stagnated flow. Thus, the $h/H = 1/3$ plate retains a certain amount of two-dimensionality, but the side source-like regions are definitely a three-dimensional feature. Those regions are probably related to the vortices which are formed in the front of the plate, adjacent to the side walls, and represent the carryover of the vortices.

For the $h/H = 1/2$ plate, both of the patterns displayed in the middle diagrams were observed, with the lower of the two being encountered somewhat more frequently. A common feature of both diagrams is a central vertical stagnation zone, from which streamlines issue more or less horizontally; that is, there is a sidewise flow. In the upper of the two

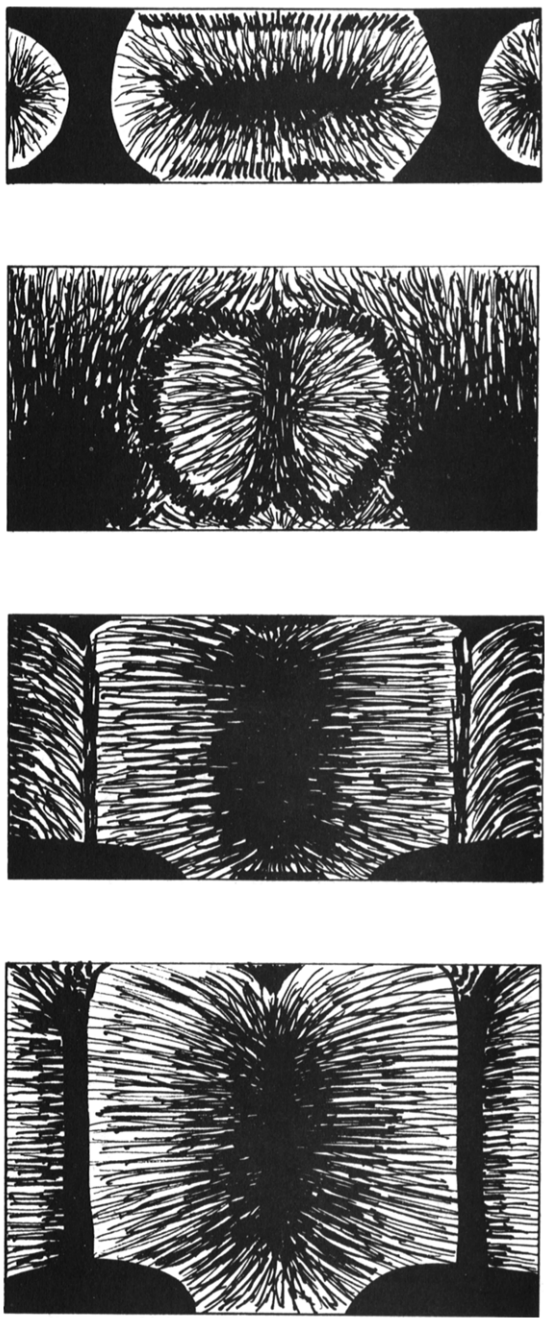

FIG. 6. Flow patterns on the downstream face of the blockage, top to bottom, $h/H = 1/3$. 1/2, 1/2 and 2/3.

diagrams, there is a ring-like stagnation region which bounds the outflow zone, but beyond that the pattern defies interpretation.

The lower of the two diagrams for $h/H = 1/2$ is more regular and is more readily rationalized. There is a sharply etched sidewise flow issuing from the central stagnation zone. It is likely that this flow is driven by the sidewise pressure gradient that is set up on the upstream face of the plate. Adjacent to the side walls, there is a zone of predominately sidewise flow, but directed oppositely to that in the inner region. This wall-adjacent sidewise flow is believed to be caused by the carryover of the vortices from the upstream face. The collision of the two opposite directed sidewise flows yields the two narrow vertical stagnation lines.

In view of the two different patterns for the $h/H = 1/2$ plate, it may be regarded as a transition case between the quasi two-dimensional pattern for $h/H = 1/3$ and the strongly three-dimensional pattern for $h/H = 2/3$.

The latter is shown in the lowermost diagram of Fig. 6. It is seen to be very similar to the neighboring flow pattern for $h/H = 1/2$, and the rationalization offered for the latter continues to apply.

In the view of the authors, the flow pattern displayed by the lower two diagrams of Fig. 6 is truly remarkable, especially the fact that the flow which sweeps the downstream face of the plate is essentially sidewise flow. The recirculation zone in which produces such a pattern must have a character altogether different from that pictured in the upper diagram of Fig. 2 (two-dimensional flow). In particular, instead of recirculating about a horizontal axis, as in Fig. 2, the recirculating flow of Fig. 6, lower diagrams, must have a vertical axis. These flows are, clearly, of great complexity.

Dimensionless parameters

In view of the analogy between the two processes, the phrases heat transfer and mass transfer will be used interchangeably. Average mass-transfer coefficients K were separately evaluated for the upstream and downstream faces of the blockage element. This was possible because, in any given data run, a naphthalene coating was applied to only one of the faces.

From measurements of the mass of the blockage element made before and after a data run, the average rate of mass transfer $\dot{m}$ per unit area was evaluated by making use of the duration time for the run and the surface area of the coating. The mass transfer is driven by the difference between the naphthalene vapor concentrations at the plate surface and in the approach flow, ρ_{nw} and ρ_{nb}, respectively. The former was evaluated from the Sogin vapor pressure–temperature relation [4] in conjunction with the perfect gas law, while the latter is zero. Thus,

$$K = \dot{m}/\rho_{nw}. \tag{1}$$

The dimensionless form of the mass-transfer coefficient is the Sherwood number, Sh, which is analogous to the Nusselt number. As is the case with the Nusselt number, it is necessary to select a characteristic dimension for the Sherwood number. Two Sherwood numbers will be employed here

$$Sh_H = KH/\mathscr{D}, \quad Sh_h = Kh/\mathscr{D} \tag{2}$$

where $\mathscr{D}$ is the mass diffusion coefficient. The first of these is based on the duct side wall dimension H (equal to the hydraulic diameter), while the second is based on the blockage height h.

The flow field will be characterized by one of three Reynolds numbers, depending on the message to be conveyed. One of these is the duct Reynolds number

$$Re_{\text{duct}} = \bar{u}H/\nu \tag{3}$$

where $\bar{u}$ is the mean velocity in the unobstructed duct. The second is a Reynolds number based on the duct mean velocity $\bar{u}$ and the blockage height h

$$\bar{u}h/\nu. \tag{4}$$

The last of the Reynolds numbers is based on the blockage height h and on the mean velocity in the gaps above and below the blockage element

$$\bar{u}_{\text{gaps}}h/\nu \tag{5}$$

where

$$\bar{u}_{\text{gaps}} = \dot{w}/\rho(H^2 - hH) \tag{5a}$$

and $\dot{w}$ is the mass flow rate of the air.

The mass-transfer analogue of the Prandtl number is the Schmidt number. The Schmidt number for sublimation of naphthalene into air is 2.5 [4]. To generalize the present results to be applicable to other Prandtl or Schmidt numbers, a power-law may be used (e.g. $Sh \sim Sc^{1/3}$ or $Nu \sim Pr^{1/3}$).

Heat-(mass-) transfer results

The presentation of the heat-(mass-) transfer results will have three foci. The first is to present the heat-transfer coefficients as such, using dimensionless groups which do not involve variable geometrical factors. Next, correlations will be attempted using alternative dimensionless groups. Finally, comparisons will be made of upstream- and downstream-face results and also with the literature.

The upstream-face heat-transfer coefficients are first plotted in the form of Sh_H (or Nu_H) vs Re_{duct}, as presented in Fig. 7. Since H is a constant in all the experiments, variations in Sh_H directly reflect variations in the heat-transfer coefficient. Furthermore, variations in Re_{duct} are caused only by changes in the mean velocity $\bar{u}$ of the flow approaching the blockage. Thus, Fig. 7 shows how the heat-transfer coefficient responds to changes in the velocity of the approach flow for different blockage heights h/H. The curves passing through the data are least-squares fits of the equation

$$Sh_H = C_1 Re_{\text{duct}}^m \tag{6}$$

where $C_1 = 2.86$, 2.12, 2.82 and 1.50, and $m = 0.522$, 0.529, 0.489, and 0.552 for $h/H = 1/6$, 1/3, 1/2, and 2/3.

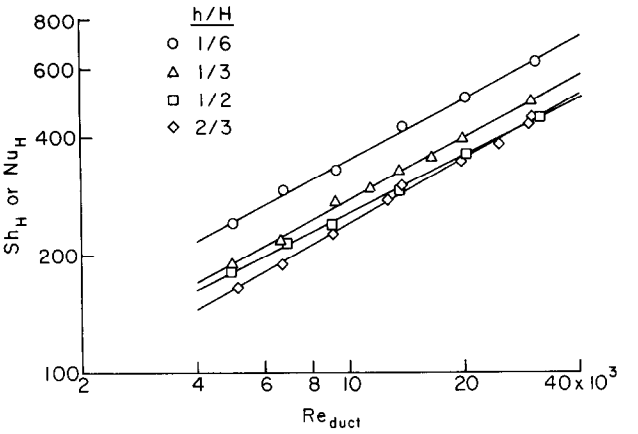

FIG. 7. Upstream-face heat-transfer coefficients, Sh_H or Nu_H vs Re_{duct}.

As expected, the heat-transfer coefficient increases with the velocity of approach. In addition, the slopes of the curves are in the range of the half power, which is conventional for stagnation-type flows. The results for the smallest blockage stand apart from the others, and this may be due to the fact that this blockage has quasi two-dimensional flow characteristics while the other blockages are more strongly three dimensional. Indeed, there seems to be a trend for Sh_H to decrease as the three-dimensional effects intensify.

The slope of the curve for $h/H = 1/2$ seems not to fit well with the others. The data runs for this case were repeated after a six-month interval and after recalibration of the analytical balance used to measure the mass of the blockage elements. The data reproduced themselves to within 2% or better. The only apparent explanation of the imperfect fit of the $h/H = 1/2$ curve with the others is that the flow transition that is in evidence adjacent to the downstream face (see Fig. 6) affected the flow adjacent to the upstream face.

The heat-transfer coefficients for the downstream face are presented in Fig. 8 using the Sh_H (or Nu_H) and Re_{duct} groupings that were used in Fig. 7. Curves have been faired through the data to provide continuity. In addition, the figure contains data from [3] that will be discussed shortly. From an inspection of Fig. 8, it is evident that the downstream-face results are less regular than are those for the upstream face. This is probably a reflection of the complex flow field adjacent to the downstream face. The results for $h/H = 1/6$ and 1/3 are especially perplexing in that there is no ready explanation of why the Sh_H values for $h/H = 1/3$ are substantially higher than the others and why the $h/H = 1/6$ data soar for Re_{duct} values greater than 10^4.

The greatest degree of regularity is evidenced by the curves for $h/H = 1/2$ and 2/3, and the Sh_H values for the former show no indication of the two different flow regimes illustrated in Fig. 6. Correlation of the results for the two largest blockage ratios will be briefly delayed to enable a single correlation to be given for both.

Attention will now be turned to the correlation of the results. For the upstream face, taking guidance from the literature, it is appropriate to seek a correlation in which the (projected) height h of the blockage serves as the characteristic dimension and $\bar{u}$ (the mean approach velocity) is the characteristic

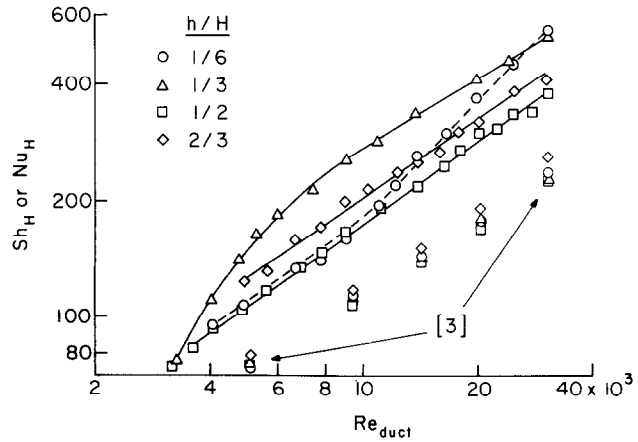

FIG. 8. Downstream-face heat-transfer coefficients, Sh_H or Nu_H vs Re_{duct}.

velocity. The data, after being rephrased in terms of Sh_h and $\bar{u}h/\nu$, have been plotted in Fig. 9.

By comparing Fig. 9 with Fig. 7, it is seen that the use of the new groupings has brought the data together to some extent. Whereas the overall vertical spread of the data in Fig. 7 was about 50%, the corresponding spread is 30% in Fig. 9. The ordering of the data with h/H has also been reversed in the two figures. The straight lines appearing in Fig. 9 are least-squares fits of the form

$$Sh_h = C_2(\bar{u}h/\nu)^m \tag{7}$$

where $C_2 = 1.22$, 1.26, 1.98, and 1.25, respectively for $h/H = 1/6$, 1/3, 1/2, and 2/3. The exponents m are the same as those for equation (6).

In seeking a correlation of the data for the downstream face, it appeared reasonable to define the Reynolds number as $\bar{u}_{gaps}h/\nu$ [equation (5)]. This selection reflects the expectation that the mean velocity in the gaps above and below the blockage plays a greater role in driving the recirculating flow than does the duct mean velocity. A plot of the downstream-face data in terms of Sh_h vs $\bar{u}_{gaps}h/\nu$ is presented in Fig. 10. In general, this figure is much tidier than is Fig. 8, where the same data were presented in terms of simpler groupings (i.e. dimensionless heat-transfer coefficient vs dimensionless duct mean velocity).

In particular, the data for the two larger blockages, $h/H = 1/2$ and 2/3, have been brought together in Fig. 10 and have been fitted with the equation

$$Sh_h = 0.184(\bar{u}_{gaps}h/\nu)^{0.698}. \tag{8}$$

The slope of this line very closely approximates the value 2/3 which is commonly encountered for fully

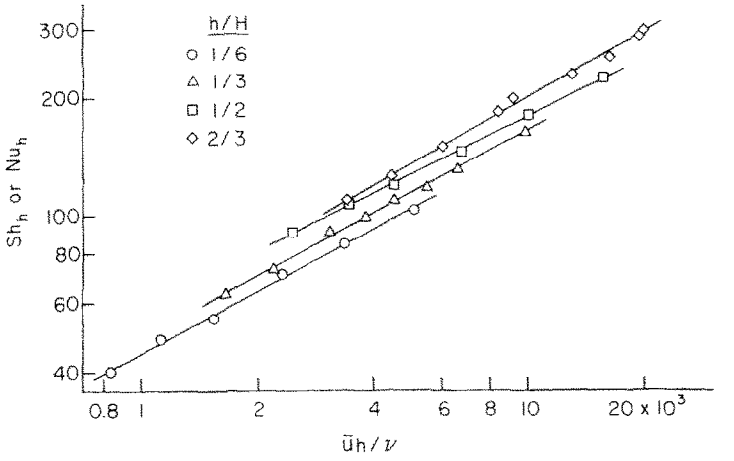

FIG. 9. Upstream-face heat-transfer coefficients, Sh_h or Nu_h vs $\bar{u}h/\nu$.

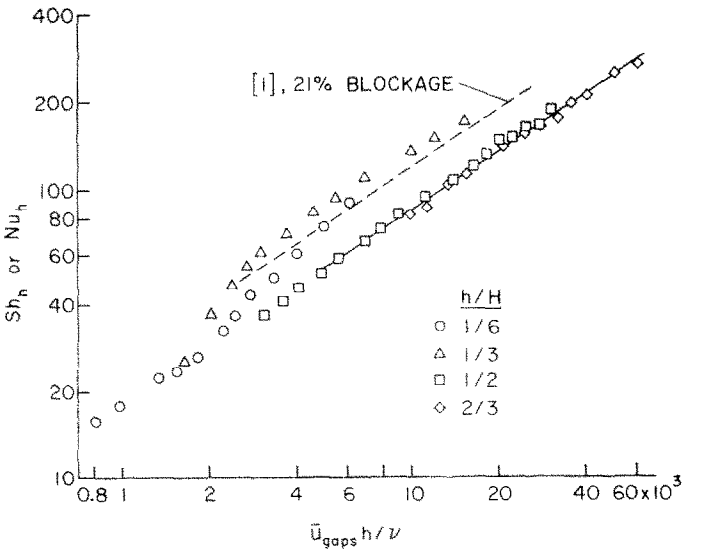

FIG. 10. Downstream-face heat-transfer coefficients, Sh_h or Nu_h vs $\bar{u}_{gaps}h/\nu$.

separated flows. The fact that the $h/H = 1/2$ and 2/3 results can be correlated together is suggestive of a common flow pattern. In terms of Fig. 6, this lends weight to the predominance of the lower of the two flow patterns pictured for $h/H = 1/2$.

The $h/H = 1/6$ and 1/3 data, as plotted in Fig. 10, continue to display individualistic trends and do not correlate with each other or with the other data. Furthermore, the overall vertical spread in Fig. 10, taken on a percentage basis, is actually greater than that in Fig. 8. Thus, although the data for $h/H = 1/2$ and 2/3 can be correlated by the groupings of Fig. 10, an overall correlation is not achieved. Perhaps, in view of the complexity of the flow and the rich variety of flow regimes, a general correlation is out of reach.

Comparisons will now be made of the upstream-face and downstream-face data, and this will be followed by comparisons with the literature. The data for the upstream and downstream faces have been brought together in Fig. 11, where it is plotted in the form Sh_H (or Nu_H) vs Re_{duct}. The data for the respective blockage ratios have been separated for the sake of clarity. Also, since the data points have already been shown in earlier figures, they are not presented in Fig. 11; rather, the data are represented by continuous faired curves (solid line for the upstream face and dashed line for the downstream face).

Figure 11 shows that the downstream face coefficients increase more rapidly with Reynolds number than do the upstream-face coefficients. This trend is consonant with literature information which indicates that separated flows yield a higher Nu vs Re slope than do unseparated flows. For the Reynolds numbers investigated, the upstream-face coefficients are higher than the downstream-face coefficients, but it is clear that a crossover is in the offing (such a crossover is already in evidence for $h/H = 1/3$). The relationship between the two sets of coefficients (i.e. degree of deviation) is not regularly ordered with h/H. This is the result of the irregular ordering of the downstream-face coefficients that was discussed earlier.

Comparisons with the literature will now be made. As noted in the Introduction, downstream-face heat-transfer experiments are reported in [1] for a plate which blocked 21% of the 22 × 32 in rectangular cross section of a wind tunnel. The experiments were performed for Reynolds numbers, based on the wind-tunnel approach velocity and plate height, in the range 10^5 to 4×10^5. These Reynolds numbers exceed those of the present investigation by more than an order of magnitude. There are numerous other differences that can be identified (rectangular vs square test section, $Pr = 0.7$ vs $Sc = 2.5$, coefficients for central region of plate vs average coefficients for entire plate). Notwithstanding these differences, the Nu, Re correlation of [1] was scaled via $Nu \sim Pr^{1/3}$, and the free stream velocity was transformed to $\bar{u}_{gaps}$. For $Pr = 2.5$, the rephrased correlation of [1] is

$$Nu_h = 0.261(\bar{u}_{gaps}h/\nu)^{2/3}. \quad (9)$$

Equation (9) has been plotted as a dashed line in Fig. 10, where the present downstream-face data are also plotted. It can be seen from the figure that equation (9) is in remarkably good agreement with the present data. The good agreement appears more noteworthy when the high-Reynolds-number origins of equation (9) are taken into consideration. The outcome of the comparison leads strong support to the present results.

Finally, the present results will be compared with those of [3], the flow configuration for which is shown

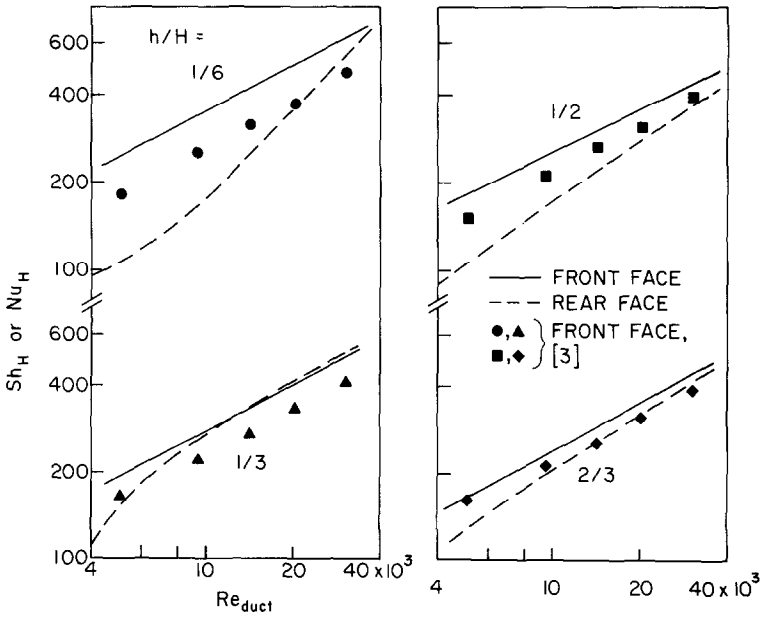

FIG. 11. Comparisons among heat-transfer coefficients.

at the right in Fig. 1. As noted in the Introduction, there are major fluid-flow differences which result from the present central positioning of the blockage and the wall attachment of the blockage in [3]. The wall-attachment stabilizes the wake downstream of the plate, and this suggests that the downstream-face heat-transfer data of [3] will be more regular than the present data, but smaller in magnitude. These expectations are borne out by the comparisons shown in Fig. 8. Depending on the blockage ratio, the heat-transfer coefficients for the wall-attached case can fall to half of those for the central blockage.

The upstream-face data of [3] are compared with the present results in Fig. 11 and are seen also to fall low, but to a substantially lesser extent than the downstream-face data. As h/H increases, the deviations between the two sets of data diminish.

CONCLUDING REMARKS

The flow visualization studies performed here afforded insights into the use of the oil-lampblack technique in addition to revealing the patterns of fluid flow adjacent to the blockage element. In general, as the blockage height increases, the flow becomes increasingly three dimensional. On the upstream face, three stagnation zones are in evidence. The downstream face is washed by highly complex recirculating flows. At higher blockages, the recirculation moves sidewise (along the span of the blockage), and two such sidewise streams collide to create a stagnation zone.

The upstream-face heat-transfer coefficients generally increase with the half power of the Reynolds number; the coefficients are higher at smaller blockages at a given duct mass flow. The sensitivity of the dimensionless results to blockage height was diminished but not eliminated when the height was used as the characteristic dimension in the Nusselt and Reynolds numbers.

The downstream-face coefficients display a complex dependence on both the blockage height and the Reynolds number. Correlation of the results for the two largest blockages was achieved by using the blockage height as the characteristic dimension and the gap velocity as the characteristic velocity. The upstream-face coefficients generally exceeded those for the downstream face, but the latter increase more rapidly with the Reynolds number.

By comparing with the results of [3], it was found that the heat-transfer coefficients for a centrally positioned blockage are larger than those for a wall-attached blockage. For the downstream face, the differences can be as large as a factor of two.

Acknowledgement — The research reported here was performed under the auspices of the National Science Foundation. The suggestions of Dr. M. Faghri at the initiation of the research are greatly appreciated.

REFERENCES

1. H. H. Sogin, A summary of experiments on local heat transfer from the rear of bluff obstacles to a low speed airflow, *J. Heat Transfer* **86**, 200–202 (1964).
2. H. H. Sogin and V. S. Subramanian, Local mass transfer from circular cylinders in cross flow, *J. Heat Transfer* **83**, 483–493 (1961).
3. E. M. Sparrow and K. P. Wachtler, Transfer coefficients on the surfaces of a transverse plate situated in a duct flow, *Int. J. Heat Mass Transfer* **21**, 761–767 (1978).
4. H. H. Sogin, Sublimation from discs to air streams flowing normal to their surfaces, *Trans. Am. Soc. Mech. Engrs* **80**, 61–71 (1958).

COEFFICIENTS DE TRANSFERT THERMIQUE TURBULENT ET CONFIGURATIONS D'ECOULEMENTS SUR LES FACES D'UN OBSTACLE POSITIONNE AU CENTRE D'UNE CONDUITE

Résumé — On conduit des expériences sur le transfert thermique et sur la visualisation de l'écoulement turbulent dans une conduite carrée dont la section droite est partiellement obstruée par un obstacle disposé au centre. Des coéfficients de convection sont obtenus à la fois pour les faces amont et aval de l'obstacle. La visualisation par la technique du noir de fumée révèle la présence de trois zones d'arrêt sur la face amont. La face aval est balayée par des zones très complexes de récirculation, caractérisées par des mouvements latéraux de fluide (dans le sens de l'envergure de l'obstacle). Les coéfficients de convection sur la face avant croissent généralement comme la racine carrée du nombre de Reynolds; pour un débit massique donné, des coefficients plus élevés sont décelés pour des hauteurs faibles d'obstacle. Les coefficients sur la face arrière montrent une dépendence compliquée à la fois de la hauteur de l'obstacle et du nombre de Reynolds. En général, pour le domaine de nombre de Reynolds considéré, les coefficients en aval sont supérieurs à ceux en amont. Des comparaisons avec la bibliographie montre que les coefficients pour un obstacle positionné au centre sont par rapport à un obstacle attaché à une paroi environ deux fois plus grands.

WÄRMEÜBERGANGSKOEFFIZIENTEN UND STRÖMUNGSFORMEN AN DEN STIRNSEITEN EINES ZENTRAL ANGEORDNETEN HINDERNISSES IN EINEM KANAL BEI TURBULENTER DURCHSTRÖMUNG

Zusammenfassung — Für turbulente Strömung durch einen quadratischen Kanal, dessen Querschnitt durch ein zentral angebrachtes Hindernis teilweise blockiert ist, wurden Wärmeübergangsmessungen durchgeführt und die Strömung sichtbar gemacht. Es wurden Wärmeübergangskoeffizienten für die in Zu- und Abströmrichtung orientierten Querschnitte des Hindernisses ermittelt. Die Sichtbarmachung der Strömung, die mit Hilfe der Öl-Ruß-Methode durchgeführt wurde, zeigte, daß auf dem Anströmquerschnitt drei Stauzonen vorhanden sind.

Der Abströmquerschnitt wird in höchst komplizierten Rezirkulations-Zonen umströmt, die durch seitliche Flüssigkeitsbewegungen über die Breite des Hindernisses gekennzeichnet sind. Die Wärmeübergangskoeffizienten am Anströmquerschnitt nehmen im allgemeinen mit der Wurzel der

Reynolds-Zahl zu; bei einem vorgegebenen Massenstrom zeigen sich größere Koeffizienten, wenn das Hindernis kleiner ist. Die Koeffizienten des Abströmquerschnitts lassen eine komplizierte Abhängigkeit sowohl von der Höhe des Hindernisses als auch von der Reynolds-Zahl erkennen. Ganz allgemein sind für den untersuchten Bereich der Reynolds-Zahl die Koeffizienten am Anströmquerschnitt größer als auf der Rückseite. Ein Vergleich mit der Literatur zeigt, daß die Koeffizienten für ein zentral angeordnetes Hindernis diejenigen für ein an der Wand angebrachtes um mindestens den Faktor zwei überschreiten.

КОЭФФИЦИЕНТЫ ТУРБУЛЕНТНОГО ПЕРЕНОСА ТЕПЛА И ХАРАКТЕР ТЕЧЕНИЯ ЖИДКОСТИ НА ТОРЦЕВЫХ ПОВЕРХНОСТЯХ ЗАГРОМОЖДАЮЩЕЙ ВСТАВКИ, РАСПОЛОЖЕННОЙ ПО ЦЕНТРУ КАНАЛА

Аннотация — Проведено экспериментальное исследование переноса тепла и характера турбулентного течения в квадратном канале, поперечное сечение которого частично загромождено вставкой, расположенной по центру канала. Определены коэффициенты теплопереноса для обеих торцевых поверхностей вставки. В результате визуализации потока методом закопченного стекла установлено наличие трех зон торможения на поверхности, расположенной вверх по потоку. У поверхности вниз по потоку отмечаются очень сложные рециркуляционные зоны, характеризующиеся растеканием жидкости в стороны по ширине вставки. Значения коэффициентов теплопереноса на поверхности вверх по потоку обычно увеличиваются как корень квадратный из числа Рейнольдса; при заданном значении потока массы наблюдаются более высокие значения коэффициентов при более низких значениях высоты загромождающей вставки. Коэффициенты теплообмена поверхности вниз по потоку зависят сложным образом как от высоты вставки, так и от числа Рейнольдса. В исследованном диапазоне значений числа Рейнольдса значения коэффициентов теплообмена поверхности, расположенной вверх по потоку, как правило, превышают значения коэффициентов поверхности, расположенной вниз по потоку. Сравнение с опубликованными данными показало, что значения коэффициентов теплообмена при установлении загромождающей вставки по центру канала в два раза выше значений этих коэффициентов при наличии загромождающей вставки на стенке канала.